ACS OMEGA

Article

Cite This: ACS Omega 2019, 4, 14780−14789

http://pubs.acs.org/journal/acsodf

Tunable Redox Potential, Optical Properties, and Enhanced Stability of Modified Ferrocene-Based Complexes

Avishek Paul,[†] Raffaele Borrelli,[‡] Houssny Bouyanfif,[§] Sébastien Gottis,[†] and Frédéric Sauvage*[,†]

[†]Laboratoire de Réactivité et Chimie des Solides CNRS UMR 7314 and [§]Laboratoire de Physique de la Matière Condensée (EA2081), Université de Picardie Jules Verne, 33 Rue Saint Leu, Amiens 80039, France

[‡]Dipartimento di Scienze Agrarie, Forestali e Alimentari, Università di Torino, Largo Paolo Braccini, 2, Grugliasco I-10095, Turin, Italy

Supporting Information

ABSTRACT: We report a series of ferrocene-based derivatives and their corresponding oxidized forms in which the introduction of simple electron donating groups like methyl or *tert*-butyl units on cyclopentadienyl-rings afford great tunability of Fe^{+III}/Fe^{+II} redox potentials from +0.403 V down to −0.096 V versus saturated calomel electrode. The spin forbidden d−d transitions of ferrocene derivatives shift slightly toward the blue region with an increasing number of electron-donating groups on the cyclopentadienyl-rings with very little change in absorptivity values, whereas the ligand-to-metal transitions of the corresponding ferricinium salts move significantly to the near-IR region. The electron-donating groups also contribute in the strengthening of electron density of Fe^{+III} d-orbitals, which therefore improves the chemical stability against the oxygen reaction. Further, density functional theory calculations show a reducing trend in outer shell reorganization energy with an increasing number of the electron donating units.

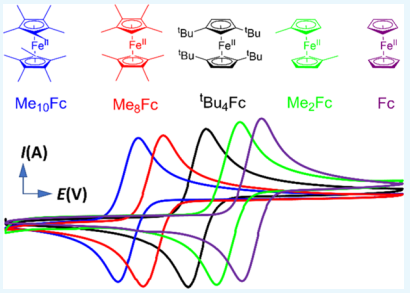

INTRODUCTION

Ferrocene is a well-known organometallic redox mediator, which has a number of applications in almost all fields related to electrochemistry.[1] The sandwich structure of ferrocene is based on two negatively charged aromatic cyclopentadienyl (Cp) rings which creates a stable 18-electron system for Fe(+II) ions.[2] It confers to the complex a high temperature robustness up to 400 °C in air,[1a,3] a reversible electrochemical characteristic at a redox potential of +0.403 V [vs saturated calomel electrode (SCE)] for which this latter is independent of the solvent properties, and good solubility in most of the common organic solvents. However, ferrocene is predisposed to various electrophilic attacks because of the electron-rich aromatic Cp-rings.[1a,4] Taking this as an advantage, it can thus serve as a potential precursor for synthesizing a variety of derivatives to finely reach the targeted asset. Ferrocene is also being used in the design of novel ligand architectures for the synthesis of various metal catalysts,[5] suitable redox couples in mixed valence states,[6,7] redox shuttles in catalysis,[8] and for the development of electrochemically active dendrons, dendrimers, and polymers.[1a,9−11] Ferrocene can be used as part of a battery electrode material[12] and has been proposed as a fast redox mediator in dye-sensitized solar cells to decrease energy losses related to the dye regeneration step.[13]

This paper reports a complete study on the characterization and density functional theory (DFT) calculations of four differently modified ferrocenes by means of the introduction of methyl and tertiary-butyl units to the Cp-rings. This study provides an insight, how and to which extent the characteristics of ferrocene can be controlled or tuned with the introduction of a simple electron donating unit to the Cp-rings. The increased electron density on the Cp-rings further influences the overall electrochemical and optical properties of the whole molecule. The consequences in terms of electrochemistry, stability, optical and magnetic properties are herein discussed.

RESULTS AND DISCUSSION

The electrochemical properties of all the ferrocene derivatives were evaluated by cyclic voltammetry (CV). All the Fe^{+III}/Fe^{+II} redox potentials and their electrochemical reversibility were also investigated taking ferrocene as the standard.[4b,c] The voltammograms recorded for the different ferrocene molecules in acetonitrile are shown in Figure 1. The Fe^{+III}/Fe^{+II} redox potential for $Me_{10}Fc^{+}/Me_{10}Fc$ was observed at −0.096 V (vs SCE) compared to standard Fc^{+}/Fc at 0.403 V (vs SCE) without affecting electrochemical reversibility. The increasing number of methyl groups on the Cp-rings gradually decreases the redox potential by ca. 100 mV (one methyl group per one Cp ring), that is, +0.302 V (vs SCE) for Me_2Fc^{+}/Me_2Fc and +0.003 V for Me_8Fc^{+}/Me_8Fc. We found a linear relationship between the redox potential of the complex and the Hammett constant (σ_p) of the substituent and its total number according to the equation $E_{1/2}$ (vs SCE) = 0.403 + 0.291σ_p (Figure S1). The synthesis of Me_4Fc and Me_6Fc still revealed to be

Received: May 9, 2019
Accepted: July 24, 2019
Published: September 4, 2019

DOI: 10.1021/acsomega.9b01341
ACS Omega 2019, 4, 14780−14789

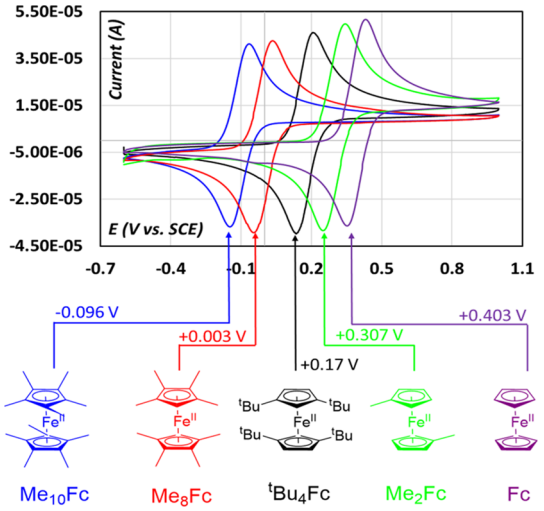

Figure 1. CV and redox potential for the Fe(III)/Fe(II) redox couple of different ferrocene derivatives. (Solvent = MeCN; supporting electrolyte = 0.1 (M) $TBAPF_6$; working electrode = glassy carbon (3 mm dia); counter electrode = Pt wire, reference electrode = SCE; scan rate = 100 mV s^{-1}).

challenging despite our efforts. Indeed, the corresponding Cp ring with two and three methyl groups (σ_p = 0.17) are found to be highly unstable and forms structural isomers during synthesis. These structural isomers revealed afterward to be rather difficult to separate also. Other synthetic routes involving the multistep methylation of a suitable ferrocene derivative (e.g., Fc or Me_2Fc) also resulted in a mixture of isomers with very low yields. As an alternative to these two complexes, we proposed the introduction of two *tert*-butyl units which has a similar Hammett constant (σ_p = 0.16) on each Cp ring, which affords lowering of the redox potential to +0.170 V (vs SCE) while keeping excellent electrochemical reversibility. This complex has been proposed by Bläser et al. and then by Gleiter et al.[18] This potential value lies exactly between Me_2Fc^+/Me_2Fc and Me_8Fc^+/Me_8Fc filling the gap with an identical synthetic procedure (Figures 1 and 2). The result is in good agreement with predicting the energetic destabilization of the iron d-orbitals within the crystal field with the increasing electron density on the Cp-rings by methyl or *tert*-butyl (^{t}Bu) groups. The greater effect of the *tert*-butyl group is due to its stronger inductive effect (σ_i = 0.07 vs 0.04 for CH_3).[19] The diffusion coefficients of these different ferrocene molecules have been determined by cyclic voltamperometry with different scan rates (Figures 2 and S2−S7). This parameter is particularly important for electrochemical applications in which the mass transport limitation can control the overall cell kinetic such as in dye-sensitized solar cells,[13c] molecular redox shuttle for batteries,[20] or as an electroactive component in redox flow batteries.[21] Randles−Sevcik equation has been utilized after verifying (i) the linear relationship between the peak currents (both anodic and cathodic) as a function of the square root of scan rate, and (ii) that the system remains rapid and reversible in the whole domain of scan rates. The obtained values of diffusion coefficients for the different complexes are reported in Table 1. Although the introduction of the methyl or *tert*-butyl group(s) onto the Cp ring will lead to a slightly more bulky complex, which can penalize its diffusion capacity into confined mesoporosity, it is however noteworthy to see a beneficial effect on the diffusion property in acetonitrile likely as a result of the increased electron density redistribution between two Cp-rings which may have improved the ion pairing interactions between ferrocene and PF_6^- ($TBAPF_6$ used as a supporting electrolyte) in the electrolyte solution. Twofold enhancement in the experimental diffusion coefficient value (from $D_{Fc} = 2.60 \times 10^{-9}$ m^2/s for ferrocene, a value in good agreement with the literature,[22] to $D_{Me_2Fc} = 5.73 \times 10^{-9}$ m^2/s for the dimethyl ferrocene counterpart) also suggests that there is a better ion pair interaction despite being heavier. More methyl groups result in a greater diffusion coefficient value, reaching as high as $D_{Me_{10}Fc^+} = 7.87 \times 10^{-9}$ m^2/s and $D_{^tBuFc^+} = 4.99 \times 10^{-9}$ m^2/s for the deca-methyl and *tert*-butyl counterparts, respectively. There are no noticeable differences on the diffusion coefficient between the ferrocene and oxidized ferricinium·TFSI derivatives except for the deca-methyl ferrocene complex regardless of the metal centers being at different oxidation states. The Fe^{+III}/Fe^{+II} redox potential values for both oxidized and reduced ferrocene molecules are almost identical. There is a slight downward shift of the whole voltamperogram compared to the parental reduced form without any significant difference in peak current or Faradaic current values (Figure 3). This downward shift was also noticed while CVs were being recorded after each successive addition of AgTFSI to the electrochemical cell in order to confirm that it is not because of any impurity (Figure S8). The reason for this downward shift of voltamperogram for oxidized forms is not very clear at the moment and needs further investigation.

Chemical and electrochemical stabilities of these complexes are other aspects while considering them to be applicable. Pure ferricinium salt is stable in the solid-state when air is excluded.

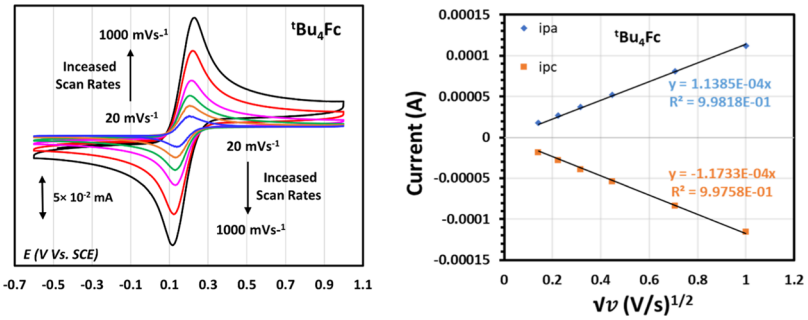

Figure 2. CV at different scan rates from 20 to 1000 mV s^{-1} of 2 mmol/L ^{t}Bu$_4$Fc in acetonitrile (supporting electrolyte: 0.1 mol/L $TBAPF_6$, glassy carbon working electrode (3 mm dia), Pt wire counter electrode, SCE as a reference electrode).

DOI: 10.1021/acsomega.9b01341
ACS Omega 2019, 4, 14780−14789

Table 1. Electrochemical and Spectroscopic Data of All Ferrocene and Ferricinium Derivatives in Acetonitrile[a]

compounds	$E_{1/2}(Fe^{3+}/Fe^{2+})$ (V)	$\Delta E_{1/2}$ (mV)	$D_{ox} \times 10^{-9}$ (m^2 s^{-1})	$D_{red} \times 10^{-9}$ (m^2 s^{-1})	D_{ox}/D_{red}	λ (nm)/ε (M^{-1} cm^{-1})
Fc[21]	+0.403	43	2.6	2.6	1	322/61
						442/95
[Fc][TFSI]	n.s.	n.s.	n.s.	n.s.	n.s.	n.s.
Me_2Fc	+0.307	56	5.73	5.94	0.96	326/59
						438/96 ± 2
[Me_2Fc][TFSI]	n.s.	n.s.	n.s.	n.s.	n.s.	386(s)
						457(s)
						552(s)
						647/97
$^tBu_4Fc$	+0.170	55	4.99	5.30	0.94	334/83
						462/105
[$^tBu_4Fc$][TFSI]	+0.170	38	4.67	4.81	0.97	390(s)
						484(s)
						597(s)
						680/370
Me_8Fc	+0.003	43	7.02	7.22	0.97	325(s)
						428/95
[Me_8Fc][TFSI]	−0.034	34	5.45	6.03	0.90	463(s)
						496(s)
						617(s)
						750/380
$Me_{10}Fc$	−0.096	46	6.47	6.71	0.96	325(s)
						423/97
[$Me_{10}Fc$][TFSI]	−0.120	44	7.37	7.87	0.94	470(s)
						518(s)
						637(s)
						698(s)
						778/488

[a]n.s. stands for not stable, s for shoulder.

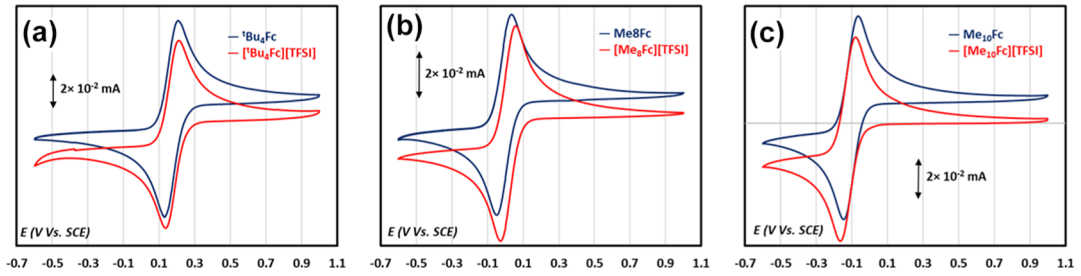

Figure 3. Difference in CV between reduced and chemically oxidized forms. (a) $^tBu_4Fc$ and $^tBu_4Fc^+$, (b) Me_8Fc and Me_8Fc^+, and (c) $Me_{10}Fc$ and $Me_{10}Fc^+$. (Solvent = MeCN; supporting electrolyte = 0.1 (M) $TBAPF_6$; working electrode = glassy carbon (3 mm dia); counter electrode = Pt wire, reference electrode = SCE; scan rate = 100 mV s^{-1}).

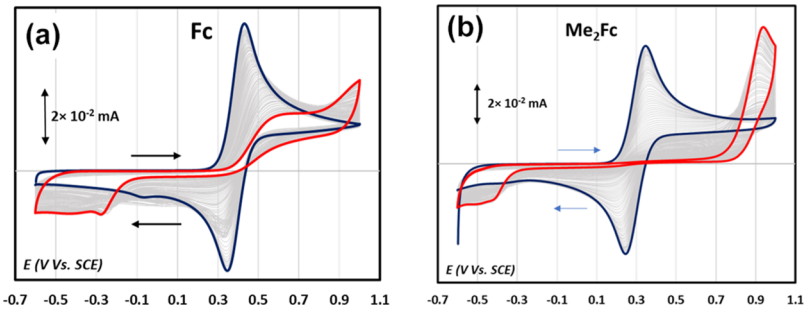

Figure 4. CV on glassy carbon electrode (3 mm dia.) in a three-electrode configuration of the 2 mM ferrocene derivative salt over 100 cycles in an acetonitrile/ambient atmosphere (supporting electrolyte: 0.1 M $TBAPF_6$, counter electrode: Pt, reference electrode: SCE, scan rate: 100 mV s^{-1}) for (a) Fc and (b) Me_2Fc.

DOI: 10.1021/acsomega.9b01341
ACS Omega 2019, 4, 14780−14789

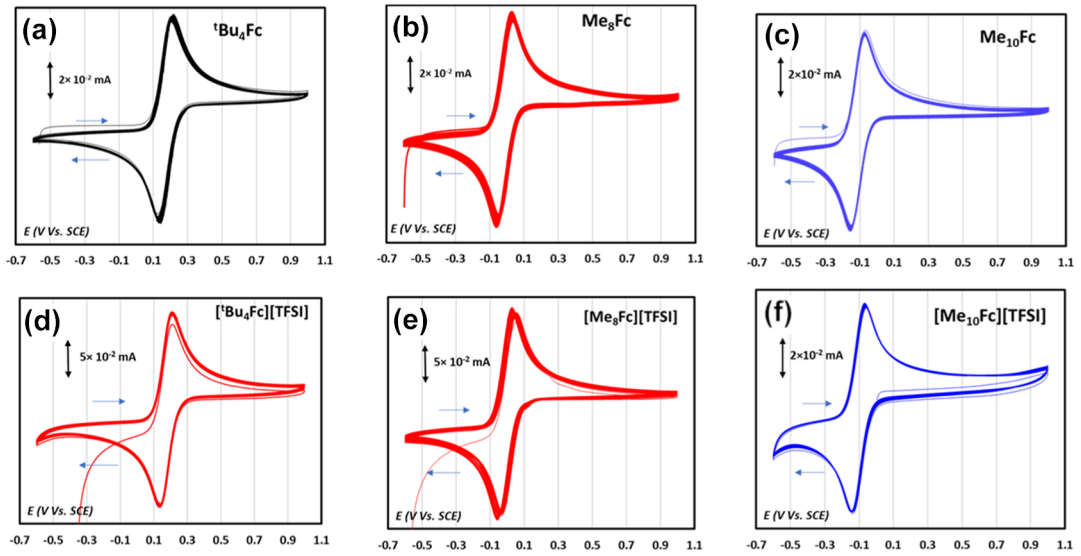

Figure 5. CV on glassy carbon electrode (3 mm dia.) in a three-electrode configuration of the 2 mM ferrocene derivative salt over 100 cycles in an acetonitrile/ambient atmosphere (supporting electrolyte: 0.1 M $TBAPF_6$, counter electrode: Pt, reference electrode: SCE, scan rate: 100 mV s^{-1}) for (a) Me_2Fc, (a) $^tBu_4Fc$, (b) Me_8Fc, (c) $Me_{10}Fc$, (d) $^tBu_4Fc^+$, (e) Me_8Fc^+, and (f) $Me_{10}Fc^+$.

However, ferricinium salt in the solution becomes unstable in de-aerated aqueous solution when the pH is lower than 4 or in de-aerated aprotic solvents. The rapid decomposition of ferrocene occurs at a pH greater than 4 or in non-aqueous solvents which can act as proton acceptors.[23] The ferricinium salt reacts with molecular oxygen in polar solvents such as acetonitrile, leading to a reactive μ-peroxy iron radical intermediate which again reacts with ferricinium salt further resulting in a μ-peroxy di-iron complex.[24] This reactivity toward oxygen is also a function of the type of counter ions and atmosphere of cycling.[25] To better assess the electrochemical stability of the different complexes in pure acetonitrile under ambient conditions, Figures 4 and 5 report the cyclic voltamperograms for ferrocene and the modified complexes including either different methyl units or *tert*-butyl groups over 100 cycles at a scan rate of 100 mV s^{-1}. Figure 4a shows that a gradual loss in peak currents and deteriorating shape of original CVs for Fc and Me_2Fc while carrying out successive oxidation/reduction cycles under ambient conditions, indicating instability of oxidized forms in solution due to a reaction with oxygen in a facile manner as described elsewhere. This is favorable to an irreversible steady-state current in oxidation and reduction, which is maintained over cycles with a large overpotential greater than 500 mV. This result highlights the rapid and continuous decomposition of electrochemically formed ferricinium after the very few first cycles. In the case of Me_2Fc, a similar decomposition of the complex is experienced (Figure 4b). However, this decomposition leads to the occurrence of an irreversible anodic faradaic peak at 0.92 V (vs SCE) and a broad steady-state cathodic current starting at −0.35 V (vs SCE) with similar features as Fc^+ except the onset, which is at a potential 200 mV greater compared to Fc^+. Interestingly, the introduction of more than one methyl or *tert*-butyl unit per Cp ring affords to greatly enhance electrochemical stability of the corresponding oxidized forms as reported in Figure 5a−f, showing a perfectly reversible fingerprint without any fading of peak currents upon cycling. This result suggests that the formation of the μ-peroxo iron radicals could have been hampered by strengthening the electron density to Fe^{+III} orbitals. The electrochemical signature and stability are similar regardless if we start by the ferrocene derivatives or the corresponding ferricinium salts obtained from chemical oxidation using AgTFSI.

The inner shell reorganization energies of the different Fc derivatives have been calculated from the fundamental definition, that is, the energy required to bring the oxidized state at the equilibrium geometry from the reduced state. This parameter is particularly important in photocatalysis and in dye-sensitized solar cells for instance because the energy requisite to undergo the "red-to-ox" reaction results in an internal energy loss of the system. In this case, the molecular geometry is first optimized for the cation (C) state and the energy $E_{cat}(C)$ is computed, then the geometry is optimized for the neutral state, one electron is removed, and the electronic energy $E_{cat}(N)$ of the cation state is computed. The reorganization energy is then defined as $\lambda_{in} = E_{cat}(N) - E_{cat}(C)$. In order to verify the accuracy and reliability of the results, the reorganization energies of Fc, Me_2Fc, and Me_8Fc have also been computed using the expression $\lambda = \frac{1}{2}\sum_n \omega_n d_n^2$, valid in the harmonic approximation of the potential energy surfaces (values reported into bracket in Table 2). Here, ω_n stands for the frequencies of the normal modes of the molecule vibration and d_n for their dimensionless displacements upon oxidation/reduction. The results, reported in Table 2, show excellent agreement between the two approaches confirming the reliability of the calculations. In all the cases, one

Table 2. Inner Shell and Outer Shell Reorganization Energies of Fc and Substituted Fc[a]

molecule	λ_{in} (meV)	λ_{out} (meV)
Fc	16(15)	780
Me_2Fc	28(22)	713
Me_8Fc	42(40)	589
$Me_{10}Fc$	42	563
$^tBu_4Fc$	46	498

[a]Values in parenthesis are obtained within the harmonic approximation. The outer shell reorganization energy is computed in acetonitrile using a two-zone heterogeneous electron-transfer model.

DOI: 10.1021/acsomega.9b01341
ACS Omega 2019, 4, 14780−14789

interesting feature of ferrocene is the niche in their very low reorganization energies which are in the order of a few tenths of meV, in agreement with previous studies on ferrocene.[26] Such a small reorganization energy is associated with minor variations of the molecular geometry upon oxidation and reduction, in contrast to polypyridyl cobalt complexes for instance used in dye-sensitized solar cells which require more than 200 meV of reorganization energy.[27] The introduction of methyl or *tert*-butyl units on Cp-rings induces only a slight increase of the reorganization energy from 16 meV for Fc to 46 meV for $^{t}Bu_4Fc$.

In addition, outer shell reorganization energy λ_o for electrode reactions have been computed considering a two-zone heterogeneous electron-transfer model[28]

$$\lambda_o = \frac{1}{2}\left(\frac{1}{\epsilon_{op}} - \frac{1}{\epsilon_{st}}\right)\left(\frac{1}{a} - \frac{1}{2d}\right)$$

where ϵ_{op} and ϵ_{st} are the optical and static dielectric constants of the solvent, a is the cavity radius of the redox species, and $2d$ is the distance between the redox species and its image in the metal electrode, that is twice the distance d of the redox species from the surface of the electrode. The effective radius a of the cavity of the redox species is obtained by using an effective value of a sphere with the same volume of the cavity obtained from the tessellation of molecular surfaces. This distance d is usually assumed to coincide with the position of the outer Helmholtz plane. This latter can be estimated as the sum of the diameter of the solvent molecule (D_{solv}) and the radius of the solvated ions (R_{ion}). The parameters used in our calculations are tabulated in Table 3.[29] In contrast to the inner reorganization energy, the introduction of methyl or *tert*-butyl groups on Cp-rings leads to a decrease of the outer-sphere reorganization energy from 780 meV for Fc to 498 meV for $^{t}Bu_4Fc$ suggesting that the modification of the pentadiene units with methyl or *tert*-butyl units affords reducing the energy of the first solvation shell.

Table 3. Parameters Used in the Calculation of the Outer-Shell Reorganization Energy[a]

ϵ_{st}	ϵ_{op}	d	D_{solv}	R_{ion}
35.688	1.806	8.31	4.31	4.00

[a]Note that the radius of the $TFSI^-$ in the electrolyte has never been reported in the literature. We assumed its size to be half of its largest atom−atom distance.

Absorption Spectra and Kinetic Study. The UV−visible absorption spectra of all ferrocene and ferricinium derivatives in acetonitrile are shown in Figure 6. Ferrocene exhibits two distinct absorption bands, at 322 nm with a very low molar extinction coefficient (ε) of 61 L mol^{-1} cm^{-1} and at 442 nm giving the typical orange color of the complex with ε = 95 L mol^{-1} cm^{-1}. The optical absorption spectrum of the ferricinium counterpart has not been determined because of fast decomposition in the solution under ambient conditions. A stronger and broad absorption band deeper in UV is also visible with a maximum at 205 nm ($\varepsilon \approx 50\,000$ L mol^{-1} cm^{-1}). This latter corresponds to an allowed $\pi-\pi^*$ transition in the Cp-rings because of its high oscillator strength ($f \approx 0.77$) in analogy with the absorption fingerprint of benzene molecules.[30] It has also some ligand-to-metal charge transfer (LMCT) characters in the red part of this band, explaining its broadness and the molar extinction coefficient dropping in the range of 8000 L mol^{-1} cm^{-1}.[31] The origin of the electronic transitions at 332 nm is still not clear from the literature.[32b−d] Indeed, it seems that the origin is not entirely a symmetry-forbidden d−d transition which occurred because of the vibrational distortion of the molecular symmetry as one could expect.[32e] Indeed, Becker et al. reported that the position of this band is independent of temperature, whereas sharpening and shifting of the band maximum with a decrease in temperature would be expected in this case.[30b] Our results show a red-shift and intensity increase of this band by the introduction of one methyl or two *tert*-butyl units in each cyclopentadienyl ring. The introduction of further methyl units leads even to a disappearance of this band or becoming curtained off by the broadening and red-shifting of the $\pi-\pi^*$ transition of Cp-rings and LMCT contribution. Consequently, this gives the credit that molecular orbitals of the rings are involved in this electronic transition at 322 nm, in agreement with Becker et al.[30b] This transition is thus assigned either to a n−π^* type symmetry-allowed transition of the type 3d-MO* or alternatively to a symmetry-forbidden $\pi-\pi^*$ transition. The band situated in the visible range at 442 nm is assigned to a forbidden d−d transition localized on the iron metal center. It is only slightly affected by the substitution on the cyclopentadienyl rings. Indeed, all ferrocene derivatives have λ_{max} at a very similar region between 442 and 423 nm, except for $^{t}Bu_4Fc$ which has λ_{max} at 462 nm. The introduction of methyl groups in the Cp core shifts therefore this optical transition to blue, signifying symmetry modification by the substitution with more localized d−d transitions on iron. The molar extinction coefficients for all the ferrocene derivatives are comparatively identical ($\varepsilon \approx 96$ L mol^{-1} cm^{-1}) except for $^{t}Bu_4Fc$ which has a slightly higher molar extinction coefficient ($\varepsilon \approx 105$ L mol^{-1} cm^{-1}). Considering the low molar extinction coefficient which

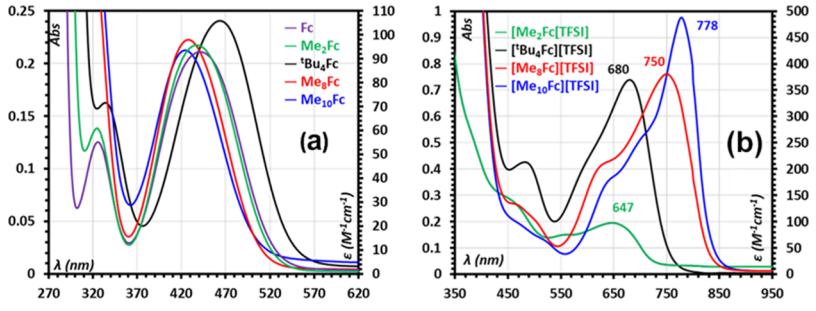

Figure 6. UV−visible absorption spectra of the different (a) ferrocene and derivatives and (b) ferricinium derivatives in acetonitrile at a concentration of 2 mmol/L.

DOI: 10.1021/acsomega.9b01341
ACS Omega 2019, 4, 14780−14789

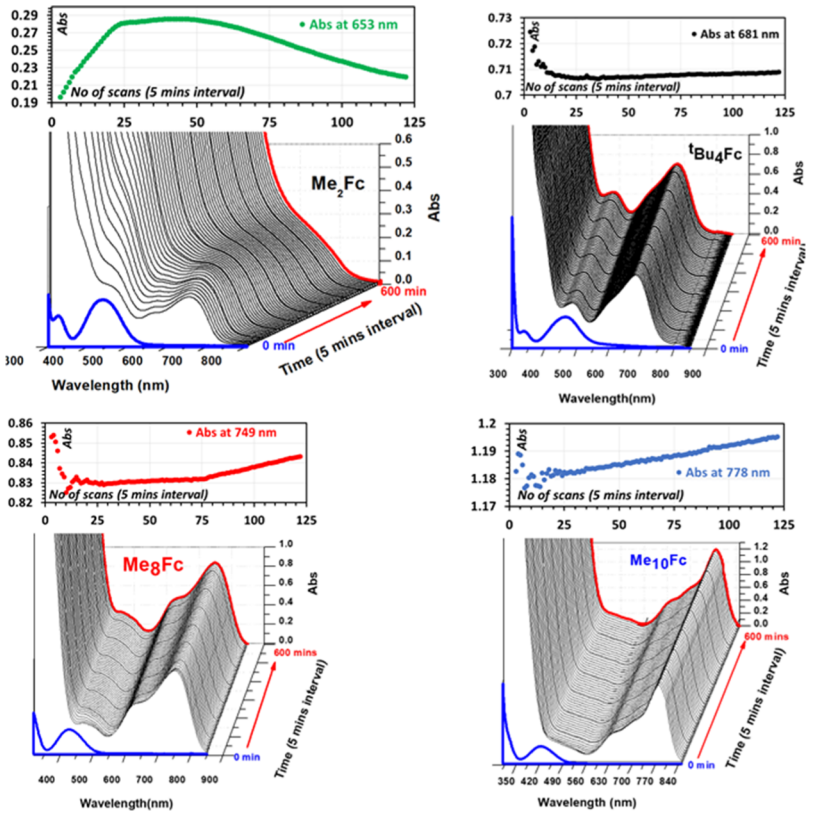

Figure 7. In situ evolution of the UV−visible absorption spectrum of 2 mmol/L solution of Me_2Fc, tBu_4Fc, Me_8Fc, and $Me_{10}Fc$ oxidation with AgTFSI in acetonitrile and stability over 10 h ageing in ambient conditions. Each spectrum was recorded at 5 min intervals. The evolution of the absorption band maximum as a function of time is reported in the inset.

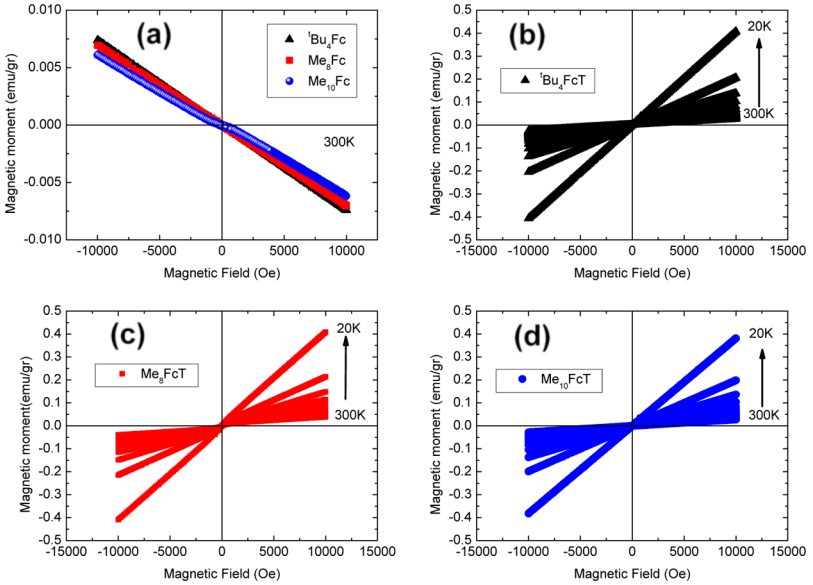

Figure 8. (a) Diamagnetic loops of the three ferrocene derivatives tBu_4Fc, Me_8Fc, and $Me_{10}Fc$ at 300 K and (b−d) paramagnetic loops as a function of temperature for $^tBu_4FcTFSI$, $Me_8FcTFSI$, and $Me_{10}FcTFSI$.

is due to the spin forbidden d−d transition, all these ferrocene derivatives absorb a very negligible amount of light in the visible region.

Regardless of the derivatives, the chemical oxidation by AgTFSI leads to a color modification of the solution turning green, which translates into a drastic modification in the absorption spectra as shown in Figure 6b. All the oxidized forms absorb part in blue up to ca. 550 nm and a stronger band for which the maximum varies more noticeably in energy from 647 nm for $[Me_2Fc][TFSI]$ to 778 nm for $[Me_{10}Fc][TFSI]$. The molar extinction coefficient is also enhanced by the substitution in the Cp-rings, for example, from 97 L mol^{-1} cm^{-1} for $[Me_2Fc][TFSI]$ to 488 L mol^{-1} cm^{-1} $[Me_{10}Fc]$-$[TFSI]$. This band is ascribed to an allowed LMCT transition

DOI: 10.1021/acsomega.9b01341
ACS Omega 2019, 4, 14780−14789

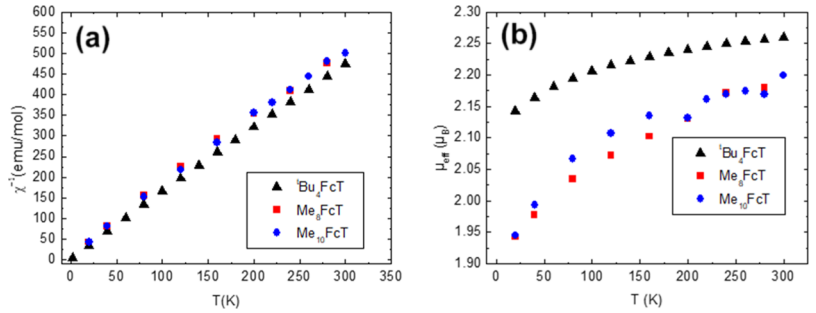

Figure 9. (a) Inverse magnetic susceptibility and (b) effective magnetic moment for the oxidized ferrocene derivatives (T = [TFSI]).

($^2E_{1u} \leftarrow {}^2E_{2g}$) in agreement with the literature.[32b−f] The reason this band is more sensitive to substitution when in the ferricinium oxidation state is explained on the basis of the d^5-Fe(III) electron configuration which leads to a more compact metal-to-ligand bonding and extended electron delocalization between the metal center and Cp-rings. The substitution in the cyclopentadienyl ring with a number of electron-donating groups, enhances the electron density in the ligand.

The chemical oxidation process for all the ferrocene derivatives was also monitored by UV−vis spectroscopy (see Figures S9−S11) with successive addition of AgTFSI. The UV−vis absorption experiment suggested a very slow oxidation process occurred for Fc → Fc^+ with AgTFSI and probably Fc being decomposed as soon as it is getting oxidized as stated elsewhere. While adding the successive amount of AgTFSI to the Me_2Fc solution in acetonitrile, it shows slow oxidation of Me_2Fc and gradual decomposition indicated by the color change from green to brown. For ferrocene, the oxidation reaction competes with the ferricinium decomposition. This is also the case for Me_2Fc to a lower extent for which the absorption value at 653 nm decreases gradually over a few hours because of the possible decomposition of Me_2Fc·TFSI in acetonitrile (Figure 7). The chemical oxidation for $^{t}Bu_4Fc$, Me_8Fc, and $Me_{10}Fc$ is almost instantaneous. The stability of the Fc^+ form has been investigated by monitoring in situ the modification of the UV−visible absorption spectrum over a period of 10 h (Figure S12). For this, the absorption value at the highest absorption peak was monitored at intervals of 5 min. The oxidized forms of $^{t}Bu_4Fc$, Me_8Fc, and $Me_{10}Fc$ show no noticeable change over 10 h demonstrating the higher stability against the oxygen reaction in good agreement with the improved reversibility in electrochemistry upon cycling (Figure 7).

Magnetic Properties. The room-temperature M(H) hysteresis loops of Fc, Me_2Fc, $^{t}Bu_4Fc$, Me_8Fc, and $Me_{10}Fc$ ferrocene derivatives are shown in Figure 8. Figures S13−S15 show an example of the hysteresis loop measured at 20 K. A negative slope is measured for all ferrocene derivatives indicating a diamagnetic behavior and the absence of unpaired electrons. The absence of unpaired electrons is in agreement with the six electrons occupying the t_{2g} levels of the d-orbitals in Fe^{+II} ions. As expected, the ferricinium derivatives exhibit a different magnetic behavior within the whole range of temperature from 300 K down to 20 K (Figure 8b−d). The linear and slight hysteresis loop is the signature of a paramagnetic behavior induced by the one unpaired electron of the Fe^{+III} metal center. In order to extract quantitative information, magnetic susceptibilities of the three oxidized compounds were estimated from the slope of the M(H) hysteresis loops. The susceptibilities were also corrected for the overall diamagnetism of the investigated oxidized substances with an approximation given by $\chi_D = -MW/2 \times 10^{-6}$ emu g^{-1}; MW denotes the molecular weight of the molecule.[33] The temperature dependence of the susceptibilities is linear with a Curie−Weiss behavior ($\chi = C/(T - \theta)$) without any hint of a magnetic phase transition. Figure 7 shows χ^{-1} and the extrapolation to $T = 0$ K of χ^{-1} gives positive values to θ reminiscent of ferromagnetic interactions between the spins (see Figures S13−S15). Effective magnetic moments were also deduced for the three oxidized derivatives $\mu_{eff} = 2.823(\chi \times T)^{1/2}$; see Miller et al. and Gray et al. for a discussion on magnetic properties and ordering in ferrocene-based complexes.[32] The expected moment value for a single spin is 1.73 μ_B. A deviation is observed for the obtained values in agreement with previous investigations on closely related molecules (Figure 8b).[34] Indeed, the obtained values depend on temperature and are in the range of 2.15−2.25 μ_B for $^{t}Bu_4Fc$·TFSI and 1.95−2.20 μ_B for Me_8Fc·TFSI and $Me_{10}Fc$·TFSI, respectively. According to Miller et al. and Reiners et al. deviation to the spin only value and temperature dependence of the effective magnetic moment is attributed to electronic excitations to higher levels, spin−orbit coupling and lower symmetry (Figure 9).[32,34]

CONCLUSIONS

A series of ferrocene-based compounds and their corresponding oxidized derivatives were synthesized and characterized by optical, electrochemical, and magnetic means. The introduction of electron-donating groups on the Cp-rings affords to lower the redox potential to a greater extent from +0.403 V for Fc^+/Fc down to −0.096 V (vs SCE) for $Me_{10}Fc^+$/$Me_{10}Fc$ without drastically increasing the reorganization energy between -red and -ox forms, remaining well below 50 meV showing high structural robustness upon electron transfer. This modification offers a substantial enhancement in the chemical/electrochemical stability of the oxidized forms in acetonitrile under ambient conditions. The introduction of methyl or *tert*-butyl groups on Cp-rings hampers the complex decomposition against oxygen reaction. Finally, our results show that the chemical modification of the Cp-ring leads to a slight blue-shift of the main absorption band for the reduced forms related to the spin forbidden d−d transition. However, a significant red-shift and molar extinction coefficient enhancement occurred for the oxidized forms related to the LMCT band.

EXPERIMENTAL SECTION

Materials. All solvents were purchased from Sigma-Aldrich and were of reagent grade except for dried tetrahydrofuran (THF) which was at 99.9% purity. Ferrocene (Fc) and 1,1′-

DOI: 10.1021/acsomega.9b01341
ACS Omega 2019, 4, 14780−14789

dimethylferrocene (Me_2Fc) were purchased from Fisher Scientific. Bis(η^5-pentamethylcyclopentadienyl)iron(II) ($Me_{10}Fc$) was purchased from Acros Organics. AgTFSI, 2,3,4-tetramethyl-1,3-cyclopentadiene, 1,2,3,4-tetramethyl-1,3-cyclopentadiene,1,3-ditertiarybutylcyclopetadiene, 1.9 mol/L *t*-BuLi in pentane, and 3 mol/L *n*-BuLi solution in hexane were purchased from Sigma-Aldrich. ^{1}H, and ^{13}C NMR spectra were recorded on a Bruker 400 MHz ADVANCE III HD spectrometer at 400 and 100 MHz, respectively. When necessary, assignments of ^{1}H and ^{13}C signals were performed using correlation spectroscopy and heteronuclear single quantum correlation. High-resolution electrospray mass spectra (HRMS) in the positive ion mode were obtained on a Q-Tof Ultima Global hybrid quadrupole/time-of-flight instrument.

Synthesis of Me_8Fc. 2.47 mL (2 g, 16.35 mmol) of 2,3,4,5-tetra methylcyclopentadienyl was taken in 20 mL THF under Ar and at 0 °C. 10 mL (18 mmol) of *n*-BuLi (1.9 mol/L in pentane) was slowly added to the reaction mixture over a period of 30 min in agreement with the literature.[14] A white slurry was obtained at the end of *n*-BuLi addition. The reaction was further allowed to stir for another 30 min. 1.28 g (7.89 mmol) of $FeCl_2$ was then added to this slurry followed by gentle heating of the reaction mixture to room temperature (20 °C). The stirring was continued for another 1 h at room temperature under Ar. The reaction mixture was then quenched by the dropwise addition of ice-cold water. Once quenched, 50 mL of extra water was added. THF was evaporated by a rotary evaporator followed by the solvent extraction of the aqueous reaction mixture with hexane (100 mL × 3). The organic layer was dried over $MgSO_4$ and a yellow-color product was collected by evaporating the solvent with a yield of 1.9 g (6.37 mmol, 81%).

Synthesis of $^tBu_4Fc$. $^tBu_4Fc$ was synthesized following rigorously the same synthetic procedure as for Me_8Fc in agreement with the literature.[14] 2 mL (1.67 g, 9.37 mmol) of bis(tertiarybutyl)cyclopentadienyl, 3.70 mL (9.37 mmol) of *n*-BuLi (2.5 M in hexane), and 593.19 mg of $FeCl_2$ were taken for the reaction. Yield: 3 g (7.49 mmol, 80%).

Synthesis and Structural Characterization of Fc, Me_2Fc, Me_8Fc, $Me_{10}Fc$, and $^tBu_4Fc$. Fc, Me_2Fc and $Me_{10}Fc$ are commercially available. Me_8Fc and $^tBu_4Fc$ were synthesized. Each ferrocene derivative was fully characterized by their melting points, NMR and high-resolution mass spectrometry and results are gathered in ESI materials.

Oxidation Procedure for [Me_2Fc][TFSI], [$^tBu_4Fc$][TFSI], [Me_8Fc][TFSI], and [$Me_{10}Fc$][TFSI]. 200 mg of each ferrocene derivatives were reacted with one equivalent of AgTFSI (silver trifluorosulfone-imide) in 20 mL of acetone under ambient conditions.[13b,15] The reaction mixture turned instantly from yellow to green. However, chemical oxidation was maintained under stirring for another 30 min at RT. The reaction mixture was then filtered through a 1 in. silica pad in order to remove the Ag particles. The crude product was collected by evaporating the solvent. The latter was further washed with hexane (10 mL × 3) to remove any unreacted ferrocene derivatives. Finally, the desired pure oxidized product was collected and dried.

Electrochemistry. All electrochemical experiments were performed using a potentiostat/galvanostat VMP3 (BioLogic Science Instruments). 100 mmol/L of $TBAPF_6$ was used as a supporting electrolyte and acetonitrile as a solvent. A 3 mm diameter glassy carbon electrode (CHI instrument) was used as a working electrode, a platinum wire as a counter electrode and a SCE as a reference electrode. All electrochemical experiments were systematically carried out using 2 mM solution the desired compound.

Absorption Spectroscopy and Kinetic Study. The UV−visible absorption spectra were recorded using an Agilent Cary 5000 UV−vis−NIR spectrophotometer in acetonitrile. Spectra were recorded in the range of 300−850 nm for the kinetic study over a period of 10 h with intervals of 5 min.

Magnetic Properties. The magnetic properties were investigated using a Cryogen Free Quantum Design system equipped with a vibrating sample magnetometer. M(H) hysteresis loops were measured under a field of up to 1 T and from 300 K down to 20 K.

Computational Details. Equilibrium geometries of all molecules in their neutral and cationic states have been optimized using DFT with the B3PW91 hybrid functional and an Ahlrichs' def2-TZVP full electron basis for all atoms including the iron center. This combination of the functional and basis set has already proven to give reliable estimates of geometry parameters for metallocenes.[16] Normal modes of vibration of Fc, Me_2Fc, and Me_8Fc have been computed at the same level of theory. The displacement of normal modes d_n have been obtained by projecting the Cartesian displacements onto the direction of normal modes by the relation[17]

$$d = \gamma^{1/2} L(x_N^0 - x_C^0)$$

where ω is the diagonal matrix of the vibrational wavenumbers in $\gamma = 2\pi\omega c/\hbar$, L is the rectangular matrix of normal modes of the neutral state expressed as linear combinations of Cartesian displacements, and $x_{N/C}^0$ are the equilibrium coordinates of the molecules in their neutral and cation states, respectively.

■ ASSOCIATED CONTENT

Supporting Information

The Supporting Information is available free of charge on the ACS Publications website at DOI: 10.1021/acsomega.9b01341.

Structural characterization of Fc, Me_2Fc, Me_8Fc, $Me_{10}Fc$, and *t*-Bu_4Fc, dependence of the redox potential as a function of the Hammett constant for the different ferrocene derivatives, CV at different scan rates from 20 to 1000 mV s^{-1} of 2 mmol/L Me_2Fc, Me_8Fc, $Me_{10}Fc$, $Bu_4FcTFSI$, $Me_8FcTFSI$, and $Me_{10}FcTFSI$ in acetonitrile and corresponding linear dependence of the faradaic anodic and cathodic peak current as a function of square root of scan rate, cyclic voltamograms of different ferrocene molecules and change after successive addition of AgTFSI, monitoring chemical oxidation of Me_2Fc, $^tBu_4Fc$, and $Me_{10}Fc$ with successive manual addition of AgTFSI using UV−visible spectroscopy, in situ evolution of the UV−visible absorption spectrum of 2 mmol/L solution of Fc, oxidation with AgTFSI in acetonitrile and stability over 10 h ageing in ambient conditions, hysteresis loops of the $^tBu_4Fc$, Me_8Fc, and $Me_{10}Fc$ derivatives from 300 K down to 20 K (PDF)

■ AUTHOR INFORMATION

Corresponding Author

*E-mail: frederic.sauvage@u-picardie.fr.

ORCID

Raffaele Borrelli: 0000-0002-0060-4520

DOI: 10.1021/acsomega.9b01341
ACS Omega 2019, 4, 14780−14789

Frédéric Sauvage: 0000-0002-7740-3209

Author Contributions

AP carried out all the synthesis, characterizations of ferrocenes, absorption properties, kinetic studies, electrochemistry, associated data processing, manuscript writing, results interpreting, and partly contributed in magnetic measurement. R.B. carried out all the calculations related to reorganization energies for ferrocene molecules. H.B. carried out the magnetic study, associated data processing, and manuscript writing. S.G. contributed in assistance for synthesis and manuscript correction. F.S. contributed in experiment design, planning, in result interpreting, manuscript writing, and correcting.

Notes

The authors declare no competing financial interest.

■ ACKNOWLEDGMENTS

F.S. wishes to acknowledge the financial support of the ANR "VISION-NIR" under the grant agreement ANR-17-CE05-0037-01 and H2020 "IMPRESSIVE" LC-SC3-RES-2-2018 under the grant agreement number 826013. F.S. wishes also to thanks Dr. David Mathiron for HRMS measurements and Dr. Gwladys Pourceau for NMR analysis, reading, and discussions.

■ REFERENCES

(1) (a) Astruc, D. Why is Ferrocene so Exceptional? *Eur. J. Inorg. Chem.* **2016**, 6−29. (b) Werner, H. At Least 60 Years of Ferrocene: The Discovery and Rediscovery of the Sandwich Complexes. *Angew. Chem., Int. Ed.* **2012**, *51*, 6052−6058.

(2) (a) Kealy, T. J.; Pauson, P. L. A New Type of Organo-Iron Compound. *Nature* **1951**, *168*, 1039. (b) Miller, S. A.; Tebboth, J. A.; Tremaine, J. F. 114. Dicyclopentadienyliron. *J. Chem. Soc.* **1952**, 632−635.

(3) Bhattacharjee, A.; Rooj, A.; Roy, D.; Roy, M. Thermal Decomposition Study of Ferrocene [(C5H5)2Fe]. *J. Exp. Phys.* **2014**, *2014*, 1.

(4) (a) Pauson, P. L.; Sandhu, M. A.; Watts, W. E.; Haley, R. C.; Knox, G. R. Ferrocene derivatives. Part XVIII. The aminomethylation of methyl- and dimethyl-ferrocene. *J. Chem. Soc. C* **1967**, 1851−1853. (b) Batterjee, S. M.; Marzouk, M. I.; Aazab, M. E.; El-Hashash, M. A. The electrochemistry of some ferrocene derivatives: redox potential and substituent effects. *Appl. Organomet. Chem.* **2003**, *17*, 291−297. (c) Silva, M. E. N. P. R. A.; Pombeiro, A. J. L.; Herrmann, R.; Deus, N.; Bozak, R.; Bozak, R. Redox potential and substituent effects in ferrocene derivatives: II. *J. Organomet. Chem.* **1994**, *480*, 81−90.

(5) (a) Colacot, T. J. A Concise Update on the Applications of Chiral Ferrocenyl Phosphines in Homogeneous Catalysis Leading to Organic Synthesis. *Chem. Rev.* **2003**, *103*, 3101−3118. (b) Barbaro, P.; Bianchini, C.; Giambastiani, G.; Parisel, S. L. Progress in stereoselective catalysis by metal complexes with chiral ferrocenyl phosphines. *Coord. Chem. Rev.* **2004**, *248*, 2131−2150.

(6) Connelly, N. G.; Geiger, W. E. Chemical Redox Agents for Organometallic Chemistry. *Chem. Rev.* **1996**, *96*, 877−910.

(7) (a) Richardson, D. E.; Taube, H. Mixed-valence molecules: Electronic delocalization and stabilization. *Coord. Chem. Rev.* **1984**, *60*, 107−129. (b) Launay, J.-P. Electron transfer in molecular binuclear complexes and relation with electron transport through nanojunctions. *Coord. Chem. Rev.* **2013**, *257*, 1544−1554. (c) Ceccon, A.; Santi, S.; Orian, L.; Bisello, A. Electronic communication in heterobinuclear organometallic complexes through unsaturated hydrocarbon bridges. *Coord. Chem. Rev.* **2004**, *248*, 683−724. (d) Murata, M.; Yamada, M.; Fujita, T.; Kojima, K.; Kurihara, M.; Kubo, K.; Kobayashi, Y.; Nishihara, H. Structural Conversion and Spin Separation in Bis(ferrocenylethynyl)anthraquinones Triggered by Proton-Coupled Intramolecular Electron Transfer. *J. Am. Chem. Soc.* **2001**, *123*, 12903−12904.

(8) (a) Chauvin, Y. Olefin Metathesis: The Early Days (Nobel Lecture). *Angew. Chem., Int. Ed.* **2006**, *45*, 3740−3747. (b) Studer, A.; Curran, D. P. The electron is a catalyst. *Nat. Chem.* **2014**, *6*, 765. (c) Saveant, J. M. Catalysis of chemical reactions by electrodes. *Acc. Chem. Res.* **1980**, *13*, 323−329. (d) Bunnett, J. F.; Zahler, R. E. Aromatic Nucleophilic Substitution Reactions. *Chem. Rev.* **1951**, *49*, 273−412. (e) Foo, K.; Sella, E.; Thomé, I.; Eastgate, M. D.; Baran, P. S. A Mild, Ferrocene-Catalyzed C−H Imidation of (Hetero)Arenes. *J. Am. Chem. Soc.* **2014**, *136*, 5279−5282.

(9) (a) Foucher, D. A.; Tang, B. Z.; Manners, I. Ring-opening polymerization of strained, ring-tilted ferrocenophanes: a route to high-molecular-weight poly(ferrocenylsilanes). *J. Am. Chem. Soc.* **1992**, *114*, 6246−6248. (b) Ni, Y.; Rulkens, R.; Manners, I. Transition Metal-Based Polymers with Controlled Architectures: Well-Defined Poly(ferrocenylsilane) Homopolymers and Multiblock Copolymers via the Living Anionic Ring-Opening Polymerization of Silicon-Bridged [1]Ferrocenophanes. *J. Am. Chem. Soc.* **1996**, *118*, 4102−4114. (c) Tanabe, M.; Vandermeulen, G. W. M.; Chan, W. Y.; Cyr, P. W.; Vanderark, L.; Rider, D. A.; Manners, I. Photocontrolled living polymerizations. *Nat. Mater.* **2006**, *5*, 467. (d) Rulkens, R.; Lough, A. J.; Manners, I.; Lovelace, S. R.; Grant, C.; Geiger, W. E. Linear Oligo(ferrocenyldimethylsilanes) with between Two and Nine Ferrocene Units: Electrochemical and Structural Models for Poly(ferrocenylsilane) High Polymers. *J. Am. Chem. Soc.* **1996**, *118*, 12683−12695. (e) Boott, C. E.; Lunn, D. J.; Manners, I. Versatile and controlled functionalization of polyferrocenylsilane-b-polyvinylsiloxane block copolymers using a N-hydroxysuccinimidyl ester strategy. *J. Polym. Sci., Part A: Polym. Chem.* **2015**, *54*, 245−252. (f) Heilmann, J. B.; Scheibitz, M.; Qin, Y.; Sundararaman, A.; Jäkle, F.; Kretz, T.; Bolte, M.; Lerner, H.-W.; Holthausen, M. C.; Wagner, M. A Synthetic Route to Borylene-Bridged Poly(ferrocenylene)s. *Angew. Chem., Int. Ed.* **2006**, *45*, 920−925. (g) Alkan, A.; Natalello, A.; Wagner, M.; Frey, H.; Wurm, F. R. Ferrocene-Containing Multifunctional Polyethers: Monomer Sequence Monitoring via Quantitative 13C NMR Spectroscopy in Bulk. *Macromolecules* **2014**, *47*, 2242−2249. (h) Buchmeiser, M. R. Homogeneous Metathesis Polymerization by Well-Defined Group VI and Group VIII Transition-Metal Alkylidenes: Fundamentals and Applications in the Preparation of Advanced Materials. *Chem. Rev.* **2000**, *100*, 1565−1604.

(10) (a) Casado, C. M.; Cuadrado, I.; Morán, M.; Alonso, B.; García, B.; González, B.; Losada, J. Redox-active ferrocenyl dendrimers and polymers in solution and immobilised on electrode surfaces. *Coord. Chem. Rev.* **1999**, *185*−*186*, 53−80. (b) Astruc, D. Electron-transfer processes in dendrimers and their implication in biology, catalysis, sensing and nanotechnology. *Nat. Chem.* **2012**, *4*, 255. (c) Ornelas, C.; Ruiz, J.; Belin, C.; Astruc, D. Giant Dendritic Molecular Electrochrome Batteries with Ferrocenyl and Pentamethylferrocenyl Termini. *J. Am. Chem. Soc.* **2009**, *131*, 590−601.

(11) (a) Long, B.; Liang, S.; Xin, D.; Yang, Y.; Xiang, J. Synthesis, characterization and in vitro antiproliferative activities of new 13-cis-retinoyl ferrocene derivatives. *Eur. J. Med. Chem.* **2009**, *44*, 2572−2576. (b) Jaouen, G.; Vessières, A.; Top, S. Ferrocifen type anti cancer drugs. *Chem. Soc. Rev.* **2015**, *44*, 8802−8817.

(12) (a) Ding, Y.; Zhao, Y.; Yu, G. A Membrane-Free Ferrocene-Based High-Rate Semiliquid Battery. *Nano Lett.* **2015**, *15*, 4108−4113. (b) Park, K.-S.; Schougaard, S. B.; Goodenough, J. B. Conducting-Polymer/Iron-Redox- Couple Composite Cathodes for Lithium Secondary Batteries. *Adv. Mater.* **2007**, *19*, 848−851. (c) Beladi-Mousavi, S. M.; Sadaf, S.; Walder, L.; Gallei, M.; Rüttiger, C.; Eigler, S.; Halbig, C. E. Poly(vinylferrocene)-Reduced Graphene Oxide as a High Power/High Capacity Cathodic Battery Material. *Adv. Energy Mater.* **2016**, *6*, 1600108.

(13) (a) Ponseca, C. S.; Chábera, P.; Uhlig, J.; Persson, P.; Sundström, V. Ultrafast Electron Dynamics in Solar Energy Conversion. *Chem. Rev.* **2017**, *117*, 10940. (b) Daeneke, T.; Mozer, A. J.; Kwon, T.-H.; Duffy, N. W.; Holmes, A. B.; Bach, U.; Spiccia, L. Dye regeneration and charge recombination in dye-sensitized solar cells with ferrocene derivatives as redox mediators. *Energy Environ. Sci.* **2012**, *5*, 7090. (c) Daeneke, T.; Kwon, T.-H.; Holmes, A. B.; Duffy,

DOI: 10.1021/acsomega.9b01341
ACS Omega 2019, 4, 14780−14789

N. W.; Bach, U.; Spiccia, L. High-efficiency dye-sensitized solar cells with ferrocene-based electrolytes. *Nat. Chem.* **2011**, *3*, 211.
(14) (a) Petrov, A. R.; Derheim, A.; Oetzel, J.; Leibold, M.; Bruhn, C.; Scheerer, S.; Oßwald, S.; Winter, R. F.; Siemeling, U. A Stable Planar-Chiral N-Heterocyclic Carbene with a 1,1′-Ferrocenediyl Backbone. *Inorg. Chem.* **2015**, *54*, 6657−6670. (b) Roemer, M.; Skelton, B. W.; Piggott, M. J.; Koutsantonis, G. A. 1,1′-Diacetyloctamethylferrocene: an overlooked and overdue synthon leading to the facile synthesis of an octamethylferrocenophane. *Dalton Trans.* **2016**, *45*, 18817−18821.
(15) Mochida, T.; Funasako, Y.; Ishida, M.; Saruta, S.; Kosone, T.; Kitazawa, T. Crystal Structures and Phase Sequences of Metallocenium Salts with Fluorinated Anions: Effects of Molecular Size and Symmetry on Phase Transitions to Ionic Plastic Crystals. *Chem.—Eur. J.* **2016**, *22*, 15725−15732.
(16) Latouche, C.; Palazzetti, F.; Skouteris, D.; Barone, V. High-Accuracy Vibrational Computations for Transition-Metal Complexes Including Anharmonic Corrections: Ferrocene, Ruthenocene, and Osmocene as Test Cases. *J. Chem. Theory Comput.* **2014**, *10*, 4565−4573.
(17) (a) Borrelli, R.; Peluso, A. Elementary electron transfer reactions: from basic concepts to recent computational advances. *Wiley Interdiscip. Rev.: Comput. Mol. Sci.* **2013**, *3*, 542−559. (b) Borrelli, R.; Peluso, A. Quantum Dynamics of Radiationless Electronic Transitions Including Normal Modes Displacements and Duschinsky Rotations: A Second-Order Cumulant Approach. *J. Chem. Theory Comput.* **2015**, *11*, 415−422.
(18) (a) Kuhn, N.; Jendral, K.; Boese, R.; Bläser, D. Heterocycles as Ligands, X1). — 2,2′,5,5′-Tetra-tert-butyl-1,1′-diazaferrocene − Stabilization of the Diheterometallocene Structure by Steric Shielding. *Chem. Ber.* **1991**, *124*, 89. (b) Janiak, C.; Kuhn, N.; Gleiter, R. Effects of isolobal substitution in cyclopentadienyl ligands: the azacyclopentadienyl system C,R,N. Comparative photoelectron spectra of the tetra-tert-butyl ferrocene derivatives. *J. Organomet. Chem.* **1994**, *475*, 223−227.
(19) Leo, A. *Substituent Constants for Correlation Analysis in Chemistry and Biology*; Wiley-Interscience: NY, 1979.
(20) Ates, M. N.; Allen, C. J.; Mukerjee, S.; Abraham, K. M. Electronic Effects of Substituents on Redox Shuttles for Overcharge Protection of Li-ion Batteries. *J. Electrochem. Soc.* **2012**, *159*, A1057−A1064.
(21) Hwang, B.; Park, M.-S.; Kim, K. Ferrocene and Cobaltocene Derivatives for Non-Aqueous Redox Flow Batteries. *ChemSusChem* **2015**, *8*, 310−314.
(22) Wang, Y.; Rogers, E. I.; Compton, R. G. The measurement of the diffusion coefficients of ferrocene and ferrocenium and their temperature dependence in acetonitrile using double potential step microdisk electrode chronoamperometry. *J. Electroanal. Chem.* **2010**, *648*, 15−19.
(23) Horsfield, A.; Wassermann, A. Electron spin resonance spectra of ferricinium. *J. Chem. Soc., Dalton Trans.* **1972**, 187−188.
(24) Hurvois, J. P.; Moinet, C. Reactivity of ferrocenium cations with molecular oxygen in polar organic solvents: Decomposition, redox reactions and stabilization. *J. Organomet. Chem.* **2005**, *690*, 1829−1839.
(25) (a) Buyukserin, F.; Martin, C. R. Investigation of Ferricinium Stability Inside the Constrained Geometry of Gold Nanotube Membranes via the Utilization of Argon Plasma. *Electrochim. Acta* **2016**, *188*, 619−624. (b) Nesmeyanov, A. N.; Materikova, R. B.; Getnarski, B. *Izv. Akad. Nauk SSSR, Ser. Khim.* **1965**, *4*, 731−733. (c) Popenoe, D. D.; Deinhammer, R. S.; Porter, M. D. Infrared spectroelectrochemical characterization of ferrocene-terminated alkanethiolate monolayers at gold. *Langmuir* **1992**, *8*, 2521−2530. (d) Abbott, N. L.; Whitesides, G. M. Potential-Dependent Wetting of Aqueous Solutions on Self-Assembled Monolayers Formed from 15-(Ferrocenylcarbonyl)pentadecanethiol on Gold. *Langmuir* **1994**, *10*, 1493−1497.
(26) Chidsey, C. E. D. Free Energy and Temperature Dependence of Electron Transfer at the Metal-Electrolyte Interface. *Science* **1991**, *251*, 919.
(27) Hagfeldt, A.; Boschloo, G.; Sun, L.; Kloo, L.; Pettersson, H. Dye-Sensitized Solar Cells. *Chem. Rev.* **2010**, *110*, 6595−6663.
(28) Liu, Y.-P.; Newton, M. D. Reorganization Energy for Electron Transfer at Film-Modified Electrode Surfaces: A Dielectric Continuum Model. *J. Phys. Chem.* **1994**, *98*, 7162−7169.
(29) Ghosh, S.; Horvath, S.; Soudackov, A. V.; Hammes-Schiffer, S. Electrochemical Solvent Reorganization Energies in the Framework of the Polarizable Continuum Model. *J. Chem. Theory Comput.* **2014**, *10*, 2091−2102.
(30) (a) Platt, J. R.; Klevens, H. B. Absolute Absorption Intensities of Alkylbenzenes in the 2250-1700 A. Region. *Chem. Rev.* **1947**, *41*, 301−310. (b) Scott, D. R.; Becker, R. S. Comprehensive Investigation of the Electronic Spectroscopy and Theoretical Treatments of Ferrocene and Nickelocene. *J. Chem. Phys.* **1961**, *35*, 516−531. (c) Maki, G. Ligand Field Theory of Ni(II) Complexes. II. Electronic Spectra and Structure of Some Paramagnetic Chelates. *J. Chem. Phys.* **1958**, *29*, 162−172.
(31) Fery-Forgues, S.; Delavaux-Nicot, B. Ferrocene and ferrocenyl derivatives in luminescent systems. *J. Photochem. Photobiol., A* **2000**, *132*, 137−159.
(32) (a) Miller, J. S.; Epstein, A. J.; Reiff, W. M. Ferromagnetic molecular charge-transfer complexes. *Chem. Rev.* **1988**, *88*, 201−220. (b) Gray, H. B.; Hendrickson, D. N.; Sohn, Y. S. Magnetic susceptibility study of various ferricenium and iron(III) dicarbollide compounds. *Inorg. Chem.* **1971**, *10*, 1559−1563. (c) Rowe, M. D.; Gale, R.; McCaffery, A. J. Distortion parameters of the ferricenium ion from low temperature absorption, MCD and ESR spectra. *Chem. Phys. Lett.* **1973**, *21*, 360−362. (d) Sohn, Y. S.; Hendrickson, D. N.; Gray, H. B. Electronic structure of ferricenium ion. *J. Am. Chem. Soc.* **1970**, *92*, 3233−3234. (e) Hendrickson, D. N.; Sohn, Y. S.; Duggan, D. M.; Gray, H. B. Low-temperature (4.2°K) study of the 2E1u ←2E2g band system in the electronic spectra of various ferricenium compounds. *J. Chem. Phys.* **1973**, *58*, 4666−4675. (f) Duggan, D. M.; Hendrickson, D. N. Electronic structure of various ferricenium systems as inferred from Raman, Infrared, low-temperature electronic absorption, and electron paramagnetic resonance measurements. *Inorg. Chem.* **1975**, *14*, 955−970.
(33) Bain, G. A.; Berry, J. F. Diamagnetic Corrections and Pascal's Constants. *J. Chem. Educ.* **2008**, *85*, 532−536.
(34) Reiners, M.; Baabe, D.; Schweyen, P.; Freytag, M.; Jones, P. G.; Walter, M. D. Teaching Ferrocenium How to Relax: A Systematic Study on Spin−Lattice Relaxation Processes in tert-Butyl-Substituted Ferrocenium Derivatives. *Eur. J. Inorg. Chem.* **2017**, 388−400.

DOI: 10.1021/acsomega.9b01341
ACS Omega 2019, 4, 14780−14789